PAPER

Check for updates

Transformer-based multitask learning for reaction prediction under low-resource circumstances†

Haoran Qiao,[a] Yejian Wu, [b] Yun Zhang, [b] Chengyun Zhang, [b] Xinyi Wu, [b] Zhipeng Wu, [b] Qingjie Zhao, [c] Xinqiao Wang,[b] Huiyu Li [*a] and Hongliang Duan*[bd]

Recently, effective and rapid deep-learning methods for predicting chemical reactions have significantly aided the research and development of organic chemistry and drug discovery. Owing to the insufficiency of related chemical reaction data, computer-assisted predictions based on low-resource chemical datasets generally have low accuracy despite the exceptional ability of deep learning in retrosynthesis and synthesis. To address this issue, we introduce two types of multitask models: retro-forward reaction prediction transformer (RFRPT) and multiforward reaction prediction transformer (MFRPT). These models integrate multitask learning with the transformer model to predict low-resource reactions in forward reaction prediction and retrosynthesis. Our results demonstrate that introducing multitask learning significantly improves the average top-1 accuracy, and the RFRPT (76.9%) and MFRPT (79.8%) outperform the transformer baseline model (69.9%). These results also demonstrate that a multitask framework can capture sufficient chemical knowledge and effectively mitigate the impact of the deficiency of low-resource data in processing reaction prediction tasks. Both RFRPT and MFRPT methods significantly improve the predictive performance of transformer models, which are powerful methods for eliminating the restriction of limited training data.

1 Introduction

With the growth of technology, deep learning for chemistry research has made significant contributions to various aspects, such as chemical reaction generation, yield prediction, retrosynthesis analysis, absorption, distribution, metabolism, excretion, and toxicity prediction, prediction of drug–target interaction, drug–target binding affinity, and compound–protein interaction.[1–10] For example, the Zhavoronkov group discovered effective inhibitors using an artificial intelligence method in 21 days, which is of significance to human life science.[11] Among these, deep learning methods that combine deep learning and reaction prediction have recently drawn much attention. Reaction prediction is typically regarded as a machine translation task from the viewpoint of natural language processing.[9] One of the popular machine translation models is the transformer, which is a fully-attention-based architecture.[12] This model provides strong support for chemical reaction scenarios. In previous studies, reaction prediction has achieved remarkable generalization ability.[13] Coley *et al.* refer to reaction centers as the minimum set of graph editors needed to convert reactant graphs to product graphs and treat reaction prediction as a graph transformation problem. They use a graph convolutional neural network to predict the set of atoms/bonds in the reaction center and then generate candidate products by enumerating all possible bond conformation changes within the set. Their model achieved a top-1 accuracy of 85.6% in the USPTO_MIT dataset.[14] However, their model did not consider the stereo structure, which is important for chemical reactions. Schwaller *et al.* treated chemical reaction prediction as a translation problem from reactants to products and applied the transformer model to it for the first time. In their study, the transformer model achieved a top-1 accuracy of 90.4% in the USPTO_MIT dataset.[12] The USPTO_MIT dataset used in these studies contained 480k chemical reactions, which is a huge amount of data. In real life, data for specific reaction types are often scarce. For example, Wang *et al.* focused on the Heck reaction prediction and relied on a transformer model. The datasets they obtained, however, only total 9000, which was not enough for a data-driven model. Therefore, the top-1 accuracy of the model was only 66.3%.[15] This phenomenon suggests

[a]College of Mathematics and Physics, Shanghai University of Electric Power, Shanghai 200090, China. E-mail: huiyuli@shiep.edu.cn

[b]Artificial Intelligence Aided Drug Discovery Institute, College of Pharmaceutical Sciences, Zhejiang University of Technology, Hangzhou 310014, China. E-mail: hduan@zjut.edu.cn

[c]Innovation Research Institute of Traditional Chinese Medicine, Shanghai University of Traditional Chinese Medicine, Shanghai 201203, China

[d]State Key Laboratory of Drug Research, Shanghai Institute of Materia Medica (SIMM), Chinese Academy of Sciences, Shanghai 201203, China

† Electronic supplementary information (ESI) available. See DOI: https://doi.org/10.1039/d2ra05349g

that the size of the training dataset significantly influences the performance of deep-learning algorithms. To address the issue caused by low-resource datasets, our study used reaction prediction as a vehicle to implement a multitasking fully data-driven model for a low-resource dataset problem.

Multitask learning is an approach to inductive transfer that improves generalization by using the domain data in the training signals of related tasks as an inductive bias. This is accomplished by learning multiple tasks simultaneously while using a shared representation; what is learned for one task can aid the learning of other tasks more effectively.[16] A multitask model is a combinational model with a capacity for multiple task prediction that can be simultaneously trained with data from various datasets and ultimately produce an enhanced multitask prediction.[17] There are many scenarios for multitask learning applications, such as pixel prediction, sentiment analysis, hotspot detection, and audio pattern recognition.[18–22]

This study implements a multiforward reaction prediction transformer (MFRPT) and retro-forward reaction prediction transformer (RFRPT) to demonstrate the feasibility of multitasking in chemical reaction prediction. Several classical low-resource datasets involving Baeyer–Villiger, Heck, and Chan–Lam reactions are used. Our models are trained without the aid of any reaction data from outside the dataset. Under the same conditions, our model outperformed all previous seq2seq models. Additionally, our models can estimate their uncertainty. We hope our study provides new insights into the application of the natural language processing model in chemical reactions and ease its dilemma under low-resource datasets.

2 Materials and methods

2.1 Problem description

The reaction prediction problem is a procedure of predicting precursor products resulting in the input reactants. Given the token sequence of the source product, x, the template-free reaction prediction model finds the most probable product token sequence, y, as follows:

$$\underset{y \in Y}{\operatorname{argmax}} \, p(y|x) \tag{1}$$

where y is the set of all possible reactant sequences. The likelihood, $p(y|x)$, is parametrized with seq2seq models like recurrent neural network[23] and transformer.[24–27] These models consist of an encoder that reads the product sequence and a decoder that autoregressively generates a distribution over the reactant sequence given the product. The decoding process starts from the initial token. To obtain multiple product prediction candidates, a beam search is used to generate and maintain multiple hypotheses at each decoding step.

2.2 Baseline model

The baseline model used in this study is based on the transformer architecture.[12] The model was originally constructed for neural machine translation tasks. The primary feature of this architecture is the complete removal of the recurrent neural network component, which is entirely dependent on the attention mechanism.

The transformer is a stepwise autoregressive encoder–decoder model, which consists of a combination of multi-head attention layers and a positional feed-forward layer. The multi-head attention layers in the encoder attend to the input sequence and encode it into a hidden representation. The decoder has two types of multi-head attention layers. The first is masked and only attends to the preceding outputs of the decoder. The second multi-head attention layer attends to the encoder and outputs of the initial decoder attention layer.

A multi-head attention layer has several scaled-dot attention layers running in parallel that are then concatenated. The scaled-dot attention uses three inputs: the keys, K; the values, V; and the queries, Q and computes the attention as follows:

$$\text{Attention}(Q, K, V) = \text{softmax}\left(\frac{QK^T}{\sqrt{d_k}}\right)V \tag{2}$$

The dot product of the queries and keys compute how closely these two are aligned. If the query and key are aligned, their dot product will be large and *vice versa*. Each key has a corresponding value vector, which is multiplied by the output of softmax to normalize the dot products and emphasize their largest components. The scaling factor d_k depends on the layer size. Based on its preceding outputs, the decoder queries the computed interesting features of the encoder from the input sequence.

2.3 Multitask-transformer model

Our model serves as a general framework for translating from one source language to many targets. Fig. 1 illustrates our
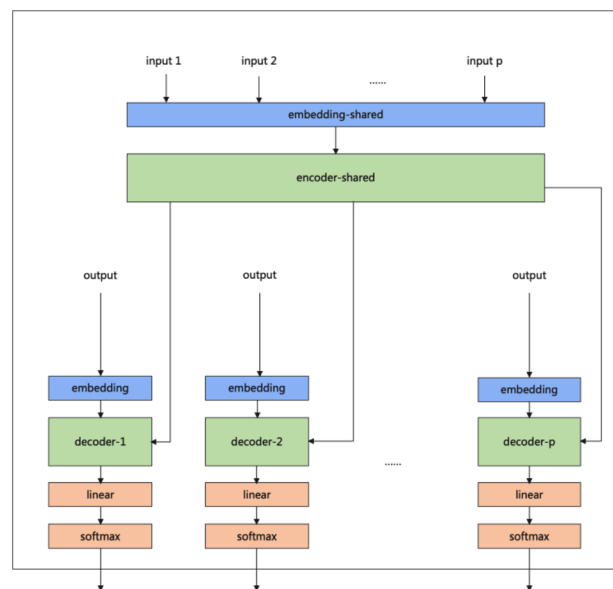

Fig. 1 Multitask transformer model architecture. Each task has a decoder and decoder-embedding. The encoder and encoder-embedding for all tasks are shared.

multitask-transformer model. The model is a transformer-based encoder–decoder architecture with multiple target tasks, each of which has a specific translation direction. Different tasks share the same translation encoder across various reaction datasets. The objective function of our multi-task model is set as the sum of multiple task likelihoods, which is the sum of several conditional probability terms conditioned on representations generated from the same encoder.

$$L(\theta) = \underset{\theta}{\text{argmax}} \sum_{T_p} \left(\frac{1}{N_p} \sum_{i}^{N_p} \log p\left(y_i^{T_p} \middle| x_i^{T_p}; \theta\right) \right) \quad (3)$$

where $\theta = \{\theta_{\text{src}}, \theta_{\text{tgt}_{T_p}}, T_p = 1, 2, ..., T_m\}$, θ_{src} is a collection of parameters for the source encoder, and $\theta_{\text{tgt}_{T_p}}$ is the parameter set of the T_p th target language. Then, N_p is the size of the parallel training corpus of the pth language pair. The target encoder parameters for different target languages are divided, allowing for the optimization of T_m.

In this study, we designed two models for different purposes according to the multitasking architecture.

(1) In the multitasking architecture, the number of tasks determines the number of decoders. MFRPT has n decoders and decoder embeddings and one encoder. For the input of n datasets, the data of the same dataset will be entered in a batch during training. During training, the data of the same dataset will be entered in one batch, and each batch will be entered into the decoder embedding to the task for the output and derive the loss to update parameter weights, while the other decoders do not update parameter weights. The test is required to specify the type of prediction reaction so that the input data into the encoder to derive the context will be input to the specified decoder. As a result, in our experiment, there are three different reaction datasets, so we trained the MFRPT with three decoders and their decoder-embedding and one encoder.

(2) We treat the reaction prediction and retrosynthesis prediction of one reaction dataset as two different tasks, with two decoders and their decoder embeddings and an encoder. We term it RFRPT. From the input point of view, only one reaction dataset is input, and the dataset is processed as forward prediction and retrosynthesis prediction (by swapping the source language and the target language) to do both tasks. In our experiments, there are three different reaction datasets, so we trained three different RFRPTs.

2.4 Datasets

In this study, we used name and structure searches from the "Reaxys" database to export Chan–Lam, Heck, and Baeyer–Villiger reaction datasets. Each dataset was preprocessed using the following procedures. First, irrelevant data (for example, pressure, temperature, and yield) were deleted from these datasets, and only reaction entries were maintained. Second, the reaction simplified molecular input line entry system (SMILES) was canonized and all duplicate reaction entries are removed. The three reaction datasets were then filtered using template screening that adheres to the respective reaction rules and the dataset was split into training, validation, and test datasets at a ratio of 8 : 1 : 1 (further details are shown in Sections S1–S3 of

the ESI†). To further demonstrate the differences between the three datasets, a dimensionality reduction algorithm called locality-sensitive hashing (LSH) forest was used to show our datasets by using TMAP. TMAP is a data visualization module designed for the visualization of molecular datasets. Schwaller *et al.* designed a reaction fingerprint and extended it to interpret chemical reactions.[28] In TMAP, reactions of the same type form a cluster and are separated from other types of reactions. Different colors are used to illustrate different reaction clusters. As shown in Fig. 2, TMAP distinguishes the three reaction types applied in our study. The three colors show the regional distribution in Fig. 2. The TMAP result demonstrates that the reaction fingerprints of the three datasets are not correlated.

2.5 Experimental details

Our models were developed using Python (version 3.8.10). A transformer model was constructed using Pytorch[29] (version 1.11) and fairseq[30] (version 0.12.2). Additionally, we used RDKit (version 2020.09.01) for reaction preprocessing and SMILES standardization. The number of encoder layers was 6, the number of decoder layers was 6, the hidden size of the positional feed-forward layers was 2048, the number of attention heads was 4. The total parameters of the baseline model were 30 million, the total parameters of RFPRT were 50 million, the total parameters of MFPRT were 70 million. A dropout probability of 0.3 was also adopted to avoid overfitting. The initial learning rate of the model was 1×10^{-3}. The Adam optimizer was used to update the learning rate, and its parameter for optimization started at 1×10^{-7}.[31] We trained for 1500 epochs using an NVIDIA RTX 3090 GPU. The source code is available online at **https://github.com/qiaohaoran/MFRPT-and-RFRPT**.

After training, each model was evaluated on the test set. The transformer is an autoregressive model. According to the vocabulary, each token in the sentence received its corresponding score. This study used a beam search to find the best results. Fig. 3 describes the time for the beam search results
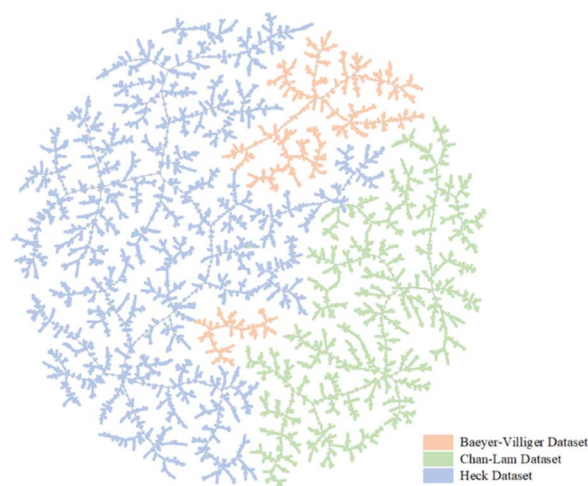

Fig. 2 TMAP plot of reaction fingerprint of reactions from datasets of three different reactions, where red is the Baeyer–Villiger reaction, blue is the Heck reaction, and yellow is the Chan–Lam reaction.
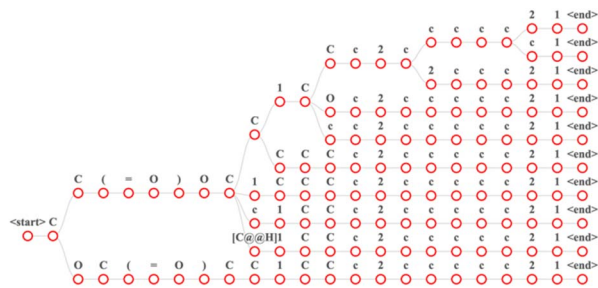
Fig. 3 Input the "CC(═O) CC1CCc2ccccc21" in the MFRPT model of beam search with a beam size of 10. In this figure, each path from the root node to the leaf node is a result.

with a beam size of 10. Each time step of the beam search produces candidate sequences based on the first N. We set the maximum decoding length to 200. If sentence decoding exceeds this length or decodes to <end> token, decoding stops. After decoding, we receive the decoded sentence, which is the output and the softmax score for each token. To calculate the top-n accuracy of each dataset, we use the decoded sentence. The top-n accuracy represents the ratio of the total number of correct outcomes predicted by the model. In "top-n," the "n" is a variable and can be all positive integers. Top-1 denotes that once the first prediction is found, the prediction results of the model scan stops. Similarly, top-2 denotes that once the first and second predictions are found, the prediction results of the model scan stops.

3 Results and discussion

3.1 Comparisons with baseline models

To discuss the performance of the MFRPT model in predicting reactions on different datasets, we show the top-n accuracies of the MFRPT model and their corresponding baseline models in Table 1. The top-1 accuracy on the Baeyer–Villiger dataset increased from 71.2% to 75.7%. For the reaction prediction on the Heck dataset, the top-1 accuracy increased from 73.3% to 81.0%, and the top-1 accuracy of reaction prediction on Chan–Lam dataset increased from 65.2% to 83.0%. After using the multitask model, the top-n accuracy of the MFRPT model in reaction prediction was significantly higher than the baseline in any top-n accuracy situation. This demonstrates that the shared

Table 1 Comparison of the performance of the baseline and MFRPT models

| Model | Dataset | Top-n accuracy (%) | | | |
		Top-1	Top-2	Top-5	Top-10
Baseline	Baeyer–Villiger	71.2	77.9	80.5	81.4
	Heck	73.3	77.5	79.4	79.7
	Chan–Lam	65.2	71.0	72.9	74.1
MFRPT	Baeyer–Villiger	75.7	80.5	81.9	82.3
	Heck	81.0	84.4	86.4	87.0
	Chan–Lam	83.0	86.0	86.7	87.5

encoder parameters can help the model learn the deeper logic contained in the SMILES, enhancing the generalization ability of the model.

Similarly, to verify the reaction prediction effect of the RFRPT model under different datasets, we show the top-1 accuracy of the three RFRPT models on three datasets and their corresponding baseline models in Fig. 4 (more detailed top-n accuracies are shown in Section S4 of the ESI†). On the Baeyer–Villiger dataset, the RFRPT model's forward reaction prediction task top-1 accuracy is 72.1% which is higher than the baseline model's 71.2%. In the retrosynthesis prediction task, the RFRPT model is 81.6% which is higher than the baseline model's 77.9%. The RFRPT's forward and retrosynthesis prediction tasks on the Heck dataset are 80.4% and 55.2%, respectively, which are higher than the baseline models' 73.3% and 37.6%, respectively. The top-1 accuracies of the Chan–Lam dataset are 78.2% and 66.5%, respectively, which are higher than the baseline models' 65.2% and 57.4%, respectively. Regarding top-1 accuracy, the RFRPT model performs better than the baseline model. In the same dataset, the RFRPT model's top-n accuracy is also higher than the baseline model. This demonstrates that the baseline model does not fully extract the chemical reaction rules from the data. Because the RFRPT model can learn from the source and target molecules, it has a good generalization ability. Despite having a lower top-n accuracy than MFRPT, RFRPT fully uses the data within a single dataset. This is a powerful way to enhance model generalization ability in low-resource situations and when there are no available data alternatives.

3.2 Error analysis

3.2.1 SMILES error. To better understand the performances of the models, we delve into the wrong predictions predicted by the baseline, RFRPT, and MFRPT models. The errors can be mainly divided into four types: SMILES error, chirality error,
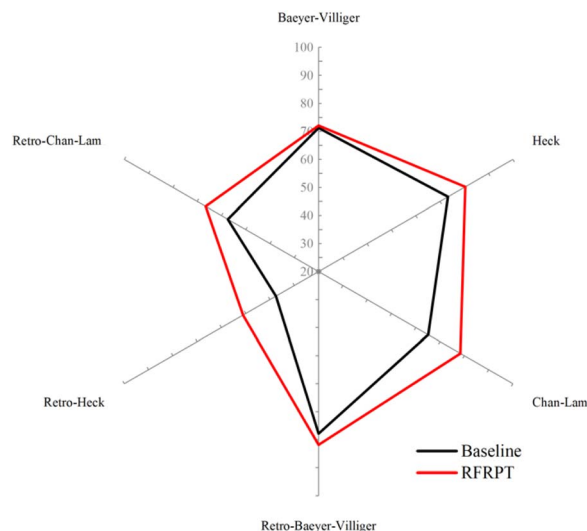

Fig. 4 Accuracies of the baseline model and retro-forward reaction prediction transformer (RFRPT) model for different reactions.

reaction site error, and other errors. As shown in Fig. 5(A), we have listed a few examples of typical SMILES errors. Invalid SMILES is a common and unavoidable problem accompanied by reaction prediction tasks using SMILES as molecular representation. To some extent, it can be said that the SMILES encoding is internally very fragile, and some cyclic or branched structures greatly increase the complexity of SMILES. Note that the RFRPT and MFRPT produce fewer wrong predictions compared to the baseline model predictions. It can be said that the two models can effectively mitigate this error by sharing more SMILES information about molecules.

3.2.2 Chirality error. Some representative examples of chiral errors are displayed in Fig. 5(B). The steric structure of a molecule is important for the properties of a drug, and differences in chiral or *cis–trans* structures may completely cause different drug effects, which is also a thorny issue in laboratories. In SMILES, the chiral center is represented by a simplified chiral identifier (@ or @@), which has no clear correspondence with the *R/S* configuration. To determine the chiral configuration of a molecule, it is necessary to first reproduce the complete molecular stereo structure with the atomic environment of the chiral atom based on the chiral identifier and then judge the configuration of this chiral center based on the groups connected around the chiral atom and the steric position it occupies. This poses an additional difficulty for the model to predict the steric structure of the product. The Baeyer–Villiger oxidation rearrangement is highly stereo-selective, and the absolute configuration of the carbon atom attached to the migrating group remains constant after undergoing the reaction, which is also one of the invisible features that the model needs to learn.

3.2.3 Reaction site error. Fig. 5(C) shows several examples of reaction site errors. As shown in Fig. 5C(a), the carbonyl groups of the reactants are flanked by benzyl and primary alkyl groups, respectively. Generally, the mobility of benzyl groups is greater than that of primary alkyl groups; therefore, the reaction tends to produce products with oxygen atoms inserted between the carbonyl and benzyl groups. For the Heck reaction, the substituent is generally added to the double-bond carbon atom with less substituent, as shown in Fig. 5C(b). Because of this, the models get confused by the multiple reaction sites in the reactants. Concerning the characteristics of reaction center and selectivity, we found that the MFRPT could learn more chemical knowledge and had a better performance by sharing chemical information.

3.2.4 Other errors. We classify some disorganized errors such as carbon number errors and missing or redundant groups as other errors. A typical example is shown in Fig. 5D(a), the four-membered ring in the product is predicted to be a five-membered ring in the baseline model and RFRPT model. A product predicted by the baseline model in Fig. 5D(b), an oxygen atom is inserted between the carbonyl and the benzene ring. These are all absurd errors that do not involve the reaction center. These errors are caused by the uniqueness of chemical information, which the models cannot recognize. However, these errors are reduced when using the MFRPT, demonstrating that MFRPT has a better ability to tackle chemical knowledge.

3.3 Uncertainty estimation of the model

It is necessary to estimate the uncertainty of the model to verify its validity. We use the logarithmic average of the probability of the model-predicted token as the confidence score to eliminate the issue of low probability caused by sentence length. We count the predictions that match the reported products and take the confidence scores above the threshold as true-positives (TPs), predictions that do not match the reported products and are below the threshold as true-negatives (TNs), predictions that match the reported products but are below the threshold as false-negatives (FNs), and finally, predictions that do not match the reported products but are above the threshold as false-positives (FPs). Further metric details are shown in Section S6 of the ESI.† Table 2 shows the results of our proposed MFRPT, RFRPT, and transformer baseline model on a full forward reaction prediction dataset. As shown in Table 2 and Fig. 6, the
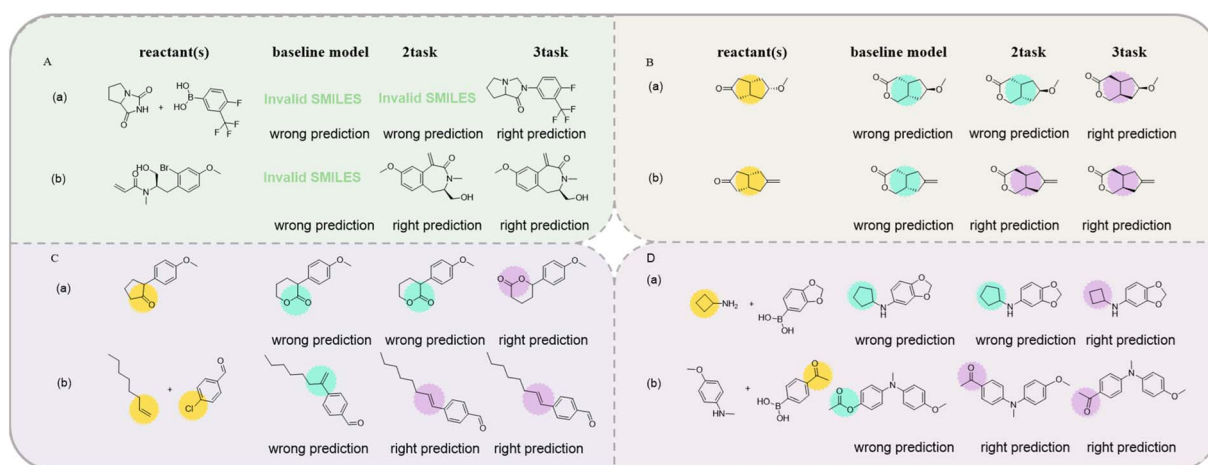

Fig. 5 Examples of the major predicted errors of the transformer model in top-1 predictions. (A) SMILES error; (B) chirality error; (C) reaction site error; (D) other error.

© 2022 The Author(s). Published by the Royal Society of Chemistry

Table 2 Comparison of the model performance of the baseline, RFRPT, and MFRPT

Model	Accuracy	Specificity	Precision	MCC	AUC
Baseline	0.803	0.667	0.860	0.527	0.774
RFRPT	0.877	0.669	0.925	0.594	0.834
MFRPT	0.883	0.620	0.931	0.551	0.818
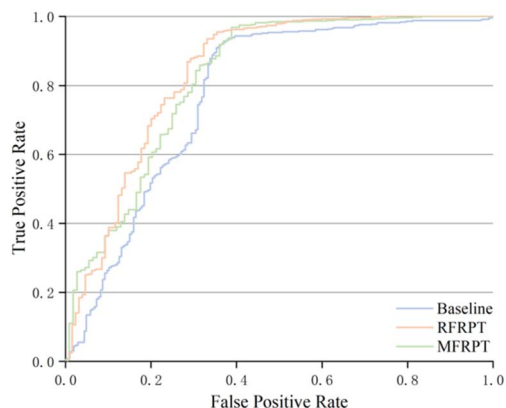
Fig. 6 ROC curve for baseline, RFRPT, and MFRPT models on full datasets when evaluated on the test set.

MFRPT model achieved the highest accuracy (0.883) and precision (0.931), but the RFRPT had the highest specificity (0.669), Matthews correlation coefficient (MCC) (0.594), and area under the receiver operating characteristic (ROC) curve (AUC) (0.834).

Fig. 6 shows the comparison results based on the ROC curves of the various models. The AUCs of RFRPT and MFRPT were 0.834 and 0.818. Compared with the baseline, the RFRPT increased the AUC by 7%.

Table 2 and Fig. 6 show that RFRPT and MFRPT are generally superior to the transformer baseline model. The RFRPT model has a better effect, and the AUC value further suggests that combining the forward reaction prediction and retrosynthesis can help the model comprehend the reaction more thoroughly, which enhances the ability of the model to discriminate. Simultaneously, the combination of various reaction datasets also enhances the reaction knowledge and qualifies the model for SMILES.

4 Conclusions

This study presents two methods: RFRPT and MFRPT for reaction prediction and retrosynthesis reaction prediction tasks based on Baeyer–Villiger, Heck, and Chan–Lam reaction datasets. Compared with the baseline model, MFRPT and RFRPT increased accuracy by 9.9% and 7%, respectively. This indicates that sharing the encoder and embedding parameters between various tasks can significantly boost the prediction performance. It also implies that the multitask framework can capture sufficient chemical knowledge and effectively address the scarcity of data in processing reaction prediction tasks.

Additionally, we conducted a deeper analysis of errors like SMILES, chirality, and regioselective that appeared in the baseline, RFRPT, and MFRPT models. Comparisons of these errors show the success of multitask framework in chemical reaction prediction. Furthermore, the uncertainty of the model is evaluated, showing that the RFRPT and MFRPT models have higher AUC than the baseline model in several indicators. The results show the efficacy of the multitask learning and transformer model and offer a useful tool for the chemical reaction prediction of small datasets. This method could be used for similar reactions and combined with other algorithms to further accelerate artificial intelligence development in reaction prediction fields.

Author contributions

All authors contributed to the study conception and design. Conceptualization, H. D.; methodology, H. Q., Y. W.; investigation, H. Q., Y. W., Y. Z.; data curation, Y. Z., X. W., X. W., Q. Z.; writing—original draft preparation, H. Q., C. Z.; writing—review and editing, H. L., Y. Z., Y. W., Z. W.; visualization, X. W., H. Q.; supervision, H. D., H. L.; funding acquisition, H. D., and all authors commented on previous versions of the manuscript. All authors read and approved the final manuscript.

Conflicts of interest

There are no conflicts to declare.

Acknowledgements

Notes and references

1 S. Moon, W. Zhung, S. Yang, J. Lim and W. Y. Kim, *Chem. Sci.*, 2022, **13**, 3661–3673.

2 S. Hu, D. Xia, B. Su, P. Chen, B. Wang and J. A. Li, *IEEE/ACM Trans. Comput. Biol. Bioinf.*, 2021, **18**, 1315–1324.

3 I. Lee and H. Nam, *J. Cheminf.*, 2022, **14**, 5.

4 H. Stark, O.-E. Ganea, L. Pattanaik, R. Barzilay and T. Jaakkola, *Presented in Part at 39th International Conference on Machine Learning (ICML 2022)*, Baltimore MD, USA, July, 2022.

5 K. Wang, R. Zhou, Y. Li and M. Li, DeepDTAF: a deep learning method to predict protein-ligand binding affinity, *Briefings Bioinf.*, 2021, **22**, bbab072.

6 S. Li, F. Wan, H. Shu, T. Jiang, D. Zhao and J. Zeng, *Cell Syst.*, 2020, **10**, 308–322.e11.

7 X. Wang, D. Liu, J. Zhu, A. Rodriguez-Paton and T. Song, *Biomolecules*, 2021, **11**, 643.

8 R. K. Bijral, I. Singh, J. Manhas and V. Sharma, *Arch. Comput. Methods Eng.*, 2022, **29**, 2513–2529.

9 V. H. Nair, P. Schwaller and T. Laino, *Chimia*, 2019, **73**, 997–1000.

10 J. Dong, M. Zhao, Y. Liu, Y. Su and X. Zeng, *Briefings Bioinf.*, 2022, **23**, bbab391.

11 A. Zhavoronkov, Y. A. Ivanenkov, A. Aliper, M. S. Veselov, V. A. Aladinskiy, A. V. Aladinskaya, V. A. Terentiev, D. A. Polykovskiy, M. D. Kuznetsov, A. Asadulaev, Y. Volkov, A. Zholus, R. R. Shayakhmetov, A. Zhebrak, L. I. Minaeva, B. A. Zagribelnyy, L. H. Lee, R. Soll, D. Madge, L. Xing, T. Guo and A. Aspuru-Guzik, *Nat. Biotechnol.*, 2019, **37**, 1038–1040.

12 A. Vaswani, N. Shazeer, N. Parmar, J. Uszkoreit, L. Jones, A. N. Gomez, Ł. Kaiser and I. Polosukhin, in *Advances in Neural Information Processing Systems 30 (NIPS 2017)*, 2017, vol. 30.

13 P. Schwaller, T. Laino, T. Gaudin, P. Bolgar, C. A. Hunter, C. Bekas and A. A. Lee, *ACS Cent. Sci.*, 2019, **5**, 1572–1583.

14 C. W. Coley, W. Jin, L. Rogers, T. F. Jamison, T. S. Jaakkola, W. H. Green, R. Barzilay and K. F. Jensen, *Chem. Sci.*, 2019, **10**, 370–377.

15 L. Wang, C. Zhang, R. Bai, J. Li and H. Duan, *Chem. Commun.*, 2020, **56**, 9368–9371.

16 R. Caruana, *Mach. Learn.*, 1997, **28**, 41–75.

17 C. Cai, S. Wang, Y. Xu, W. Zhang, K. Tang, Q. Ouyang, L. Lai and J. Pei, *J. Med. Chem.*, 2020, **63**, 8683–8694.

18 F. Rahimi, E. E. Milios and S. Matwin, in *Proceedings of the 21st ACM Symposium on Document Engineering (DocEng 2021)*, vol. 8, pp. 1–4, DOI: **10.1145/3469096.3474926**.

19 L. Ilias and D. Askounis, *IEEE J. Biomed. Health Inform.*, 2022, **26**, 4153–4164.

20 X. Zhang, S. Zhang, Z. Cui, Z. Li, J. Xie and J. Yang, *IEEE Trans. Multimed.*, 2022, DOI: **10.1109/TMM.2022.3147664**.

21 T. Zhang, X. Gong and C. L. P. Chen, *IEEE Trans. Cybern.*, 2021, **52**, 6232–6243.

22 S. Kataria, J. Villalba and N. Dehak, in *Proceedings of the 2021 IEEE International Conference on Acoustics, Speech, and Signal Processing (ICASSP 2021)*, pp. 7118–7122.

23 P. Schwaller, T. Gaudin, D. Lanyi, C. Bekas and T. Laino, *Chem. Sci.*, 2018, **9**, 6091–6098.

24 X. Wang, Y. Li, J. Qiu, G. Chen, H. Liu, B. Liao, C.-Y. Hsieh and X. Yao, *Chem. Eng. J.*, 2021, **420**, 129845.

25 E. Kim, D. Lee, Y. Kwon, M. S. Park and Y. S. Choi, *J. Chem. Inf. Model.*, 2021, **61**, 123–133.

26 I. V. Tetko, P. Karpov, R. Van Deursen and G. Godin, *Nat. Commun.*, 2020, **11**, 5575.

27 K. Mao, X. Xiao, T. Xu, Y. Rong, J. Huang and P. Zhao, *Neurocomput*, 2021, **457**, 193–202.

28 P. Schwaller, D. Probst, A. C. Vaucher, V. H. Nair, D. Kreutter, T. Laino and J.-L. Reymond, *Nat. Mach. Intell.*, 2021, **3**, 144–152.

29 A. Paszke, S. Gross, F. Massa, A. Lerer, J. Bradbury, G. Chanan, T. Killeen, Z. Lin, N. Gimelshein, L. Antiga, A. Desmaison, A. Kopf, E. Yang, Z. DeVito, M. Raison, A. Tejani, S. Chilamkurthy, B. Steiner, L. Fang, J. Bai and S. Chintala, in *Advances in Neural Information Processing Systems 32 (NIPS 2019)*, 2019, vol. 32.

30 M. Ott, S. Edunov, A. Baevski, A. Fan, S. Gross, N. Ng, D. Grangier and M. Auli, arXiv, 2019, preprint, arXiv:1904.01038, DOI: **10.48550/arXiv.1904.01038**.

31 B. Cortiñas-Lorenzo and F. Pérez-González, *Entropy*, 2020, **22**, 1379.